IV International Conference on Computational Methods for Coupled Problems in Science and Engineering
COUPLED PROBLEMS 2011
M. Papadrakakis, E. Oñate and B. Schrefler (Eds)

MULTISCALE SPACE–TIME COMPUTATION TECHNIQUES

KENJI TAKIZAWA* AND TAYFUN E. TEZDUYAR†

*Department of Modern Mechanical Engineering and
Waseda Institute for Advanced Study, Waseda University
1-6-1 Nishi-waseda, Shinjuku-ku,Tokyo 169-8050, JAPAN

†Mechanical Engineering, Rice University – MS 321
6100 Main Street, Houston, TX 77005, USA

Key words: Fluid-structure interaction, Space–time formulations, Multiscale techniques, NURBS, Space–time variational multiscale method

Abstract. A number of multiscale space–time techniques have been developed recently by the Team for Advanced Flow Simulation and Modeling (T★AFSM) for fluid–structure interaction computations. As part of that, we have introduced a space–time version of the residual-based variational multiscale method. It has been designed in the context of the Deforming-Spatial-Domain/Stabilized Space–Time formulation, which was developed earlier by the T★AFSM for computation of flow problems with moving boundaries and interfaces. We describe this multiscale space–time technique, and present results from test computations.

1 INTRODUCTION

A number of multiscale space–time techniques [1, 2, 3, 4, 5] have been developed recently by the Team for Advanced Flow Simulation and Modeling (T★AFSM) for fluid–structure interaction (FSI) computations. These have been mostly multiscale techniques based on effective ways of dealing with the different spatial or temporal scales that may be involved in the fluid and structure parts of the problem. They have been tested in conjunction with the Deforming-Spatial-Domain/Stabilized Space–Time (DSD/SST) formulation [6, 7] and stabilized space–time FSI (SSTFSI) technique [8], both developed by the T★AFSM. In addition, recently we have introduced a multiscale space–time technique [9] that is based on representing the different flow scales involved in the fluid mechanics part, so that we could have a good turbulence model for high Reynolds number flows. This multiscale technique, which we call "DSD/SST-VMST", is the space–time version of the residual-based variational multiscale method [10, 11, 12, 13, 14, 15]. The technique has also been successfully tested in 3D computations [16]. This paper is a short version of the

journal paper [9]. We describe the DSD/SST-VMST technique, and present results from test computations.

2 GOVERNING EQUATIONS AND SPACE–TIME FORMULATION OF INCOMPRESSIBLE FLOWS

2.1 Governing equations

Let $\Omega_t \subset \mathbb{R}^{n_{sd}}$ be the spatial domain with boundary Γ_t at time $t \in (0,T)$. The subscript t indicates the time-dependence of the domain. The Navier–Stokes equations of incompressible flows are written on Ω_t and $\forall t \in (0,T)$ as

$$\rho\left(\frac{\partial \mathbf{u}}{\partial t} + \boldsymbol{\nabla}\cdot(\mathbf{u}\mathbf{u}) - \mathbf{f}\right) - \boldsymbol{\nabla}\cdot\boldsymbol{\sigma} = \mathbf{0}, \tag{1}$$

$$\boldsymbol{\nabla}\cdot\mathbf{u} = 0, \tag{2}$$

where ρ, $\mathbf{u}$ and $\mathbf{f}$ are the density, velocity and the external force, respectively. The stress tensor $\boldsymbol{\sigma}$ is defined as $\boldsymbol{\sigma}(p,\mathbf{u}) = -p\mathbf{I} + 2\mu\boldsymbol{\varepsilon}(\mathbf{u})$, with $\boldsymbol{\varepsilon}(\mathbf{u}) = \left((\boldsymbol{\nabla}\mathbf{u}) + (\boldsymbol{\nabla}\mathbf{u})^T\right)/2$. Here p is the pressure, $\mathbf{I}$ is the identity tensor, $\mu = \rho\nu$ is the viscosity, ν is the kinematic viscosity, and $\boldsymbol{\varepsilon}(\mathbf{u})$ is the strain-rate tensor. The essential and natural boundary conditions Eq. (1) are represented as $\mathbf{u} = \mathbf{g}$ on $(\Gamma_t)_{\mathrm{g}}$ and $\mathbf{n}\cdot\boldsymbol{\sigma} = \mathbf{h}$ on $(\Gamma_t)_{\mathrm{h}}$, where $(\Gamma_t)_{\mathrm{g}}$ and $(\Gamma_t)_{\mathrm{h}}$ are complementary subsets of the boundary Γ_t, $\mathbf{n}$ is the unit normal vector, and $\mathbf{g}$ and $\mathbf{h}$ are given functions. A divergence-free velocity field $\mathbf{u}_0(\mathbf{x})$ is specified as the initial condition.

2.2 Space–time variational formulation

A space–time variational formulation of incompressible flows (see for example [6, 17, 18, 7]) is written over a sequence of N space–time slabs Q_n, where Q_n is the slice of the space–time domain between the time levels t_n and t_{n+1}, and P_n is the lateral boundary of Q_n. We denote the trial and test functions spaces for the velocity and pressure as $\mathbf{u} \in \mathcal{S}_{\mathbf{u}}$, $p \in \mathcal{S}_p$, $\mathbf{w} \in \mathcal{V}_{\mathbf{u}}$ and $q \in \mathcal{V}_p$. In deriving the variational formulation, we start with multiplying Eqs. (1) and (2) with the corresponding test functions, integrating them over Q_n, and setting it equal to zero:

$$\int_{Q_n} \mathbf{w}\cdot\rho\left(\frac{\partial \mathbf{u}}{\partial t} + \boldsymbol{\nabla}\cdot(\mathbf{u}\mathbf{u}) - \mathbf{f}\right) dQ - \int_{Q_n} \mathbf{w}\cdot\boldsymbol{\nabla}\cdot\boldsymbol{\sigma}\, dQ + \int_{Q_n} q\boldsymbol{\nabla}\cdot\mathbf{u}\, dQ = 0. \tag{3}$$

We integrate by parts all the terms except for the external force and enforce the essential (i.e. strong Dirichlet) and natural boundary conditions over $(P_n)_{\mathrm{g}}$ and $(P_n)_{\mathrm{h}}$, the complementary subsets of P_n. That gives us the following variational formulation: find $\mathbf{u} \in \mathcal{S}_{\mathbf{u}}$

and $p \in \mathcal{S}_p$ such that $\forall\ \mathbf{w} \in \mathcal{V}_\mathbf{u}$ and $\forall\ q \in \mathcal{V}_p$

$$\int_{\Omega_{n+1}} \mathbf{w}_{n+1}^- \cdot \rho \mathbf{u}_{n+1}^- d\Omega - \int_{\Omega_n} \mathbf{w}_n^+ \cdot \rho \mathbf{u}_n^- d\Omega - \int_{Q_n} \frac{\partial \mathbf{w}}{\partial t} \cdot \rho \mathbf{u} dQ - \int_{(P_n)_\mathrm{h}} (\mathbf{w} \cdot \rho \mathbf{u}) (\mathbf{n} \cdot \mathbf{v}) \, dP$$
$$+ \int_{(P_n)_\mathrm{h}} (\mathbf{w} \cdot \rho \mathbf{u}) (\mathbf{n} \cdot \mathbf{u}) \, dP - \int_{Q_n} \boldsymbol{\nabla} \mathbf{w} : \rho \mathbf{u} \mathbf{u} dQ - \int_{Q_n} \mathbf{w} \cdot \rho \mathbf{f} dQ - \int_{(P_n)_\mathrm{h}} \mathbf{w} \cdot \mathbf{h} dP$$
$$+ \int_{Q_n} \boldsymbol{\varepsilon}(\mathbf{w}) : \boldsymbol{\sigma} dQ + \int_{P_n} q \mathbf{n} \cdot \mathbf{u} dP - \int_{Q_n} \boldsymbol{\nabla} q \cdot \mathbf{u} dQ = 0, \tag{4}$$

where the notation $(\cdot)_n^-$ and $(\cdot)_n^+$ denotes the values at t_n as approached from below and above, and $\mathbf{v} = \frac{d\mathbf{x}}{dt}$ is the velocity of the spatial-domain boundary.

2.3 Scale separation

In the variational multiscale techniques [10, 11, 12, 13] the "coarse-scale" and "fine-scale" are separated as follows:

$$\mathcal{S}_\mathbf{u} = \overline{\mathcal{S}_\mathbf{u}} \oplus \mathcal{S}'_\mathbf{u}, \quad \mathcal{S}_p = \overline{\mathcal{S}_p} \oplus \mathcal{S}'_p, \quad \mathcal{V}_\mathbf{u} = \overline{\mathcal{V}_\mathbf{u}} \oplus \mathcal{V}'_\mathbf{u}, \quad \mathcal{V}_p = \overline{\mathcal{V}_p} \oplus \mathcal{V}'_p. \tag{5}$$

The coarse-scale part of Eq. (4) is written as follows:

$$\int_{\Omega_{n+1}} \overline{\mathbf{w}}_{n+1}^- \cdot \rho \mathbf{u}_{n+1}^- d\Omega - \int_{\Omega_n} \overline{\mathbf{w}}_n^+ \cdot \rho \mathbf{u}_n^- d\Omega - \int_{Q_n} \frac{\partial \overline{\mathbf{w}}}{\partial t} \cdot \rho \mathbf{u} dQ - \int_{(P_n)_\mathrm{h}} (\overline{\mathbf{w}} \cdot \rho \mathbf{u}) (\mathbf{n} \cdot \mathbf{v}) \, dP$$
$$+ \int_{(P_n)_\mathrm{h}} (\overline{\mathbf{w}} \cdot \rho \mathbf{u}) (\mathbf{n} \cdot \mathbf{u}) \, dP - \int_{Q_n} \boldsymbol{\nabla} \overline{\mathbf{w}} : \rho \mathbf{u} \mathbf{u} dQ - \int_{Q_n} \overline{\mathbf{w}} \cdot \rho \mathbf{f} dQ - \int_{(P_n)_\mathrm{h}} \overline{\mathbf{w}} \cdot \mathbf{h} dP$$
$$+ \int_{Q_n} \boldsymbol{\varepsilon}(\overline{\mathbf{w}}) : \boldsymbol{\sigma} dQ + \int_{P_n} \overline{q} \mathbf{n} \cdot \mathbf{u} dP - \int_{Q_n} \boldsymbol{\nabla} \overline{q} \cdot \mathbf{u} dQ = 0. \tag{6}$$

From [10, 11, 12, 13], the fine-scale solutions are represented by the strong-form residuals of the coarse-scale:

$$\mathbf{u}' = -\frac{\tau_\mathrm{M}}{\rho} \mathbf{r}_\mathrm{M} (\overline{\mathbf{u}}, \overline{p}), \tag{7}$$
$$p' = -\rho \nu_\mathrm{C} r_\mathrm{C} (\overline{\mathbf{u}}), \tag{8}$$

where

$$\mathbf{r}_\mathrm{M} (\mathbf{u}, p) = \rho \left(\frac{\partial \mathbf{u}}{\partial t} + \mathbf{u} \cdot \boldsymbol{\nabla} \mathbf{u} - \mathbf{f} \right) + \boldsymbol{\nabla} p - 2 \boldsymbol{\nabla} \cdot \mu \boldsymbol{\varepsilon}(\mathbf{u}), \tag{9}$$
$$r_\mathrm{C} (\mathbf{u}) = \boldsymbol{\nabla} \cdot \mathbf{u}, \tag{10}$$

and τ_M and ν_C are stabilization parameters measured in units of time and kinematic viscosity, respectively.

Remark 1 *More on the fine-scale approximation in conjunction with the Green's operator can be found in [10, 11, 12, 13].*

2.4 DSD/SST formulation

In the DSD/SST method [6, 17, 18, 7, 8], the space–time finite element interpolation functions are continuous within a space–time slab, but discontinuous from one space–time slab to another. The finite-dimensional trial and test functions spaces for the velocity and pressure are denoted as $\mathbf{u}^h \in \left(\mathcal{S}_{\mathbf{u}}^h\right)_n$, $p^h \in \left(\mathcal{S}_p^h\right)_n$, $\mathbf{w}^h \in \left(\mathcal{V}_{\mathbf{u}}^h\right)_n$ and $q^h \in \left(\mathcal{V}_p^h\right)_n$.

2.4.1 Fine-scale discretization

The fine-scale solutions are evaluated over each element from Eqs. (7) and (8) with $\mathbf{u}^h \in \left(\mathcal{S}_{\mathbf{u}}^h\right)_n$ and $p^h \in \left(\mathcal{S}_p^h\right)_n$:

$$\mathbf{u}' = -\frac{\tau_{\mathrm{M}}}{\rho}\mathbf{r}_{\mathrm{M}}\left(\mathbf{u}^h, p^h\right), \tag{11}$$

$$p' = -\rho\nu_{\mathrm{C}} r_{\mathrm{C}}\left(\mathbf{u}^h\right). \tag{12}$$

Remark 2 *When the polynomial order of the shape functions is less than two, the last term in Eq. (9) vanishes.*

There are various ways of defining τ_{M} and ν_{C}. For τ_{M} we use the definition

$$\tau_{\mathrm{M}} = \tau_{\mathrm{SUPG}}, \tag{13}$$

where τ_{SUPG} comes from [7], specifically the definition as given by Eqs. (107)–(109) in [7], which can also be found as the definition given by Eqs. (7)–(9) in [8]. For ν_{C}, we the consider ν_{LSIC} definition given in [8]:

$$\nu_{\mathrm{C}} = \nu_{\mathrm{LSIC}} = \tau_{\mathrm{SUPG}} \left\|\mathbf{u}^h - \mathbf{v}^h\right\|^2, \tag{14}$$

where $\mathbf{v}^h$ is the mesh velocity, and the definition from [14]:

$$\nu_{\mathrm{C}} = \left(\tau_{\mathrm{M}} \sum_{i=1}^{n_{sd}} G_{ii}\right)^{-1}, \tag{15}$$

where

$$G_{ij} = \sum_{k=1}^{n_{sd}} \frac{\partial \xi_k}{\partial x_i}\frac{\partial \xi_k}{\partial x_j}, \tag{16}$$

and $\boldsymbol{\xi}$ is the vector of element coordinates. In our computations we evaluate the stabilization parameters at $\boldsymbol{\xi} = \mathbf{0}$.

Remark 3 *The τ_{SUGN12} component of the τ_{SUPG} definition given by Eqs. (107)–(109) in [7] is the space–time version of the original definition in [19]. These definitions sense, in addition to the element geometry, the order of the interpolation functions. Some τ definitions do that and some do not. The definitions in Sections 3.3.1 and 3.3.2 of [20], for example, are among those that do not.*

Remark 4 *Remark 3 is applicable also when the interpolation functions are NURBS functions. This includes classical p-refinement and also k-refinement, except when used in conjunction with periodic B-splines.*

Remark 5 *In meshes made of NURBS, for quadrilateral (or hexahedral) elements that degenerate to triangles (or tetrahedra), we calculate τ_{SUGN12}, τ_{SUGN1} when applicable, and "h_{RGN}" embedded in the τ_{SUGN3} definition in a special way. Instead of letting the sum of the magnitudes involved in the expression degenerate, we first add together the basis functions associated with the coalescing control points, and then apply the expression using the modified basis functions. In other words, we do not degenerate the expression, but instead apply the expression to the degenerated basis functions. This special way is applicable also in the context of finite element meshes.*

2.4.2 Coarse-scale discretization

Spatially discretized version of Eq. (6) is written as follows: find $\mathbf{u}^h \in \left(\mathcal{S}^h_{\mathbf{u}}\right)_n$ and $p^h \in \left(\mathcal{S}^h_p\right)_n$ such that $\forall\ \mathbf{w}^h \in \left(\mathcal{V}^h_{\mathbf{u}}\right)_n$ and $\forall\ q^h \in \left(\mathcal{V}^h_p\right)_n$:

$$\begin{aligned}
&\int_{\Omega_{n+1}} (\mathbf{w}^h)^-_{n+1} \cdot \rho \left((\mathbf{u}^h)^-_{n+1} + (\mathbf{u}')^-_{n+1}\right) d\Omega - \int_{\Omega_n} (\mathbf{w}^h)^+_n \cdot \rho \left((\mathbf{u}^h)^-_n + (\mathbf{u}')^-_n\right) d\Omega \\
&- \int_{Q_n} \frac{\partial \mathbf{w}^h}{\partial t} \cdot \rho(\mathbf{u}^h + \mathbf{u}') dQ + \int_{(P_n)_{\mathrm{h}}} \left(\mathbf{w}^h \cdot \rho \left(\mathbf{u}^h + \mathbf{u}'\right)\right) \left(\mathbf{n}^h \cdot (\mathbf{u}^h + \mathbf{u}' - \mathbf{v}^h)\right) dP \\
&- \int_{Q_n} \boldsymbol{\nabla} \mathbf{w}^h : \rho(\mathbf{u}^h + \mathbf{u}')(\mathbf{u}^h + \mathbf{u}') dQ - \int_{Q_n} \mathbf{w}^h \cdot \rho \mathbf{f}^h dQ - \int_{(P_n)_{\mathrm{h}}} \mathbf{w}^h \cdot \mathbf{h}^h dP \\
&+ \int_{Q_n} \boldsymbol{\varepsilon}(\mathbf{w}^h) : \left(\boldsymbol{\sigma}(p^h, \mathbf{u}^h) + \boldsymbol{\sigma}'\right) dQ + \int_{P_n} q^h \mathbf{n}^h \cdot (\mathbf{u}^h + \mathbf{u}') dP \\
&- \int_{Q_n} \boldsymbol{\nabla} q^h \cdot (\mathbf{u}^h + \mathbf{u}') dQ = 0.
\end{aligned} \tag{17}$$

Here $\boldsymbol{\sigma}' \equiv \boldsymbol{\sigma} - \boldsymbol{\sigma}^h$ is introduced temporarily. We set the fine-scale solution to zero at the spatial and temporal boundaries, use the assumption $\boldsymbol{\varepsilon}(\mathbf{w}^h) : 2\mu \boldsymbol{\nabla} \mathbf{u}' = 0$ (see [12, 21]), and obtain the following form:

$$\begin{aligned}
&\int_{\Omega_{n+1}} (\mathbf{w}^h)^-_{n+1} \cdot \rho (\mathbf{u}^h)^-_{n+1} d\Omega - \int_{\Omega_n} (\mathbf{w}^h)^+_n \cdot \rho (\mathbf{u}^h)^-_n d\Omega - \int_{Q_n} \frac{\partial \mathbf{w}^h}{\partial t} \cdot \rho(\mathbf{u}^h + \mathbf{u}') dQ \\
&+ \int_{(P_n)_{\mathrm{h}}} \left(\mathbf{w}^h \cdot \rho \mathbf{u}^h\right) \left(\mathbf{n}^h \cdot (\mathbf{u}^h - \mathbf{v}^h)\right) dP - \int_{Q_n} \boldsymbol{\nabla} \mathbf{w}^h : \rho(\mathbf{u}^h + \mathbf{u}')(\mathbf{u}^h + \mathbf{u}') dQ \\
&- \int_{Q_n} \mathbf{w}^h \cdot \rho \mathbf{f}^h dQ - \int_{(P_n)_{\mathrm{h}}} \mathbf{w}^h \cdot \mathbf{h}^h dP + \int_{Q_n} \boldsymbol{\varepsilon}(\mathbf{w}^h) : \boldsymbol{\sigma}(p^h + p', \mathbf{u}^h) dQ \\
&+ \int_{P_n} q^h \mathbf{n}^h \cdot \mathbf{u}^h dP - \int_{Q_n} \boldsymbol{\nabla} q^h \cdot (\mathbf{u}^h + \mathbf{u}') dQ = 0.
\end{aligned} \tag{18}$$

2.4.3 Comparison with the original DSD/SST formulation

We can further rearrange the terms in the formulation given by Eq. (18) to compare it with the original DSD/SST formulation (with the advection term retained in the conservation-law form) and obtain the following:

$$\begin{aligned}
&\int_{Q_n} \mathbf{w}^h \cdot \rho \left(\frac{\partial \mathbf{u}^h}{\partial t} + \boldsymbol{\nabla} \cdot (\mathbf{u}^h \mathbf{u}^h) - \mathbf{f}^h \right) dQ + \int_{Q_n} \boldsymbol{\varepsilon}(\mathbf{w}^h) : \boldsymbol{\sigma}(p^h, \mathbf{u}^h) dQ - \int_{(P_n)_{\mathrm{h}}} \mathbf{w}^h \cdot \mathbf{h}^h dP \\
&+ \int_{Q_n} q^h \cdot \boldsymbol{\nabla} \mathbf{u}^h dQ + \int_{\Omega_n} (\mathbf{w}^h)_n^+ \cdot \rho \left((\mathbf{u}^h)_n^+ - (\mathbf{u}^h)_n^- \right) d\Omega \\
&- \sum_{e=1}^{(n_{el})_n} \int_{Q_n^e} \left[\rho \left(\frac{\partial \mathbf{w}^h}{\partial t} + \mathbf{u}^h \cdot \boldsymbol{\nabla} \mathbf{w}^h \right) + \boldsymbol{\nabla} q^h \right] \cdot \mathbf{u}' dQ - \sum_{e=1}^{(n_{el})_n} \int_{Q_n^e} \boldsymbol{\nabla} \cdot \mathbf{w}^h p' dQ \\
&- \sum_{e=1}^{(n_{el})_n} \int_{Q_n^e} \rho \mathbf{u}' \cdot \left(\boldsymbol{\nabla} \mathbf{w}^h \right) \mathbf{u}^h dQ - \sum_{e=1}^{(n_{el})_n} \int_{Q_n^e} \rho \mathbf{u}' \cdot \left(\boldsymbol{\nabla} \mathbf{w}^h \right) \mathbf{u}' dQ = 0.
\end{aligned} \tag{19}$$

Here each Q_n is decomposed into elements Q_n^e, where $e = 1, 2, \ldots, (n_{el})_n$. The subscript n used with n_{el} is for the general case where the number of space–time elements may change from one space–time slab to another.

Remark 6 *The last two terms correspond to the Reynolds stress and cross-stress, respectively. We call this formulation DSD/SST-VMST (i.e. the version with the variational multiscale turbulence model).*

Remark 7 *If we exclude the last two terms, the formulation is the same as the original DSD/SST formulation (with the advection term retained in the conservation-law form) under the conditions that $\tau_{PSPG} = \tau_{SUPG}$ and $\nu_{\mathrm{C}} = \nu_{LSIC}$. The 6th and 7th terms are the SUPG/PSPG and LSIC (least-squares on incompressibility constraint) stabilization terms, respectively. We name this DSD/SST-SUPS (i.e. the version with the SUPG/PSPG stabilization).*

Remark 8 *One of the main differences between the ALE and DSD/SST forms of the variational multiscale method is that the DSD/SST formulation retains the fine-scale time derivative term $\frac{\partial \mathbf{u}'}{\partial t}\big|_{\boldsymbol{\xi}}$. Dropping this term is called the "quasi-static" assumption (see [15] for the terminology). This is the same as the WTSE option in the DSD/SST formulation (see Remark 2 of [8]). We believe that this makes a significant difference, especially when the polynomial orders in space or time are higher (see Section 6 in [9]).*

3 TEST COMPUTATIONS WITH FLOW PAST AN AIRFOIL

The airfoil is NACA 64-618 and the geometry is approximated with quadratic B-splines. The computational domain is $(-5, 10) \times (-5, 5)$. The leading edge is located at $(0, 0)$.

The angle of attack is 0°. The length and velocity scales are the chord length and inflow velocity, respectively. The Reynolds number is 6.0×10^6. We compute the problem with the DSD/SST-DP-SUPS and DSD/SST-DP-VMST techniques, using the ν_{LSIC} definition given by Eq. (14) and neglecting the $2\boldsymbol{\nabla}\cdot\mu\boldsymbol{\varepsilon}(\mathbf{u})$ term in Eq. (9). With both techniques, we use two different meshes, one made of quadratic B-splines and one made of linear finite elements. First we manually generate a "frame" control mesh made of quadratic B-splines, which has 8 patches and is shown in Figure 1. Then, by a knot-insertion process that

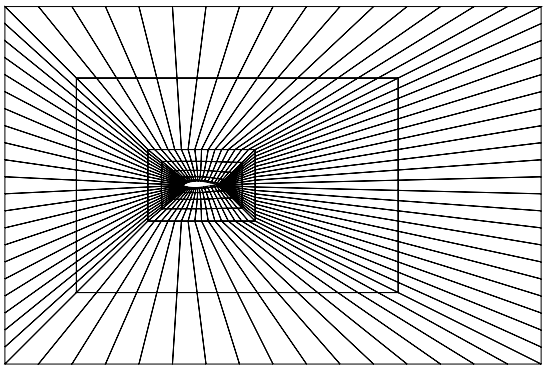

Figure 1: Frame control mesh made of quadratic B-splines. The mesh has 8 patches.

involves little manual intervention, we generate a refined control mesh made of quadratic B-splines, which has 1,681 control points and 1,400 elements. To generate the mesh made of linear finite elements, we start with a quadrilateral mesh generated by interpolating the NURBS geometry at each knot intersection. We subdivide each quadrilateral element into two triangles. The resulting mesh has 1,450 nodes and 2,780 elements. Both meshes are shown in Figure 2. The boundary conditions consist of a uniform velocity at the inflow boundary, zero stress at the outflow boundary, no-slip conditions on the airfoil, and slip conditions at the top and bottom boundaries. The time-step size is 0.01. The number of nonlinear iterations per time step is 3, with 30, 60 and 270 GMRES iterations for the first, second and third nonlinear iterations, respectively. Figures 3–6 show the pressure coefficient and velocity magnitude for the four test computations. Table 1 shows the drag and lift coefficients for the four test computations, together with the measured values from Figure 2a in [22].

4 CONCLUDING REMARKS

A number of multiscale space–time techniques have been developed recently by the T★AFSM for FSI computations, mostly multiscale techniques based on effective ways of dealing with the different spatial or temporal scales that may be involved in the fluid and structure parts of the problem. In addition, recently we have introduced a multiscale space–time technique that is based on representing the different flow scales involved in the fluid mechanics part, thus giving us a good turbulence model for high Reynolds number

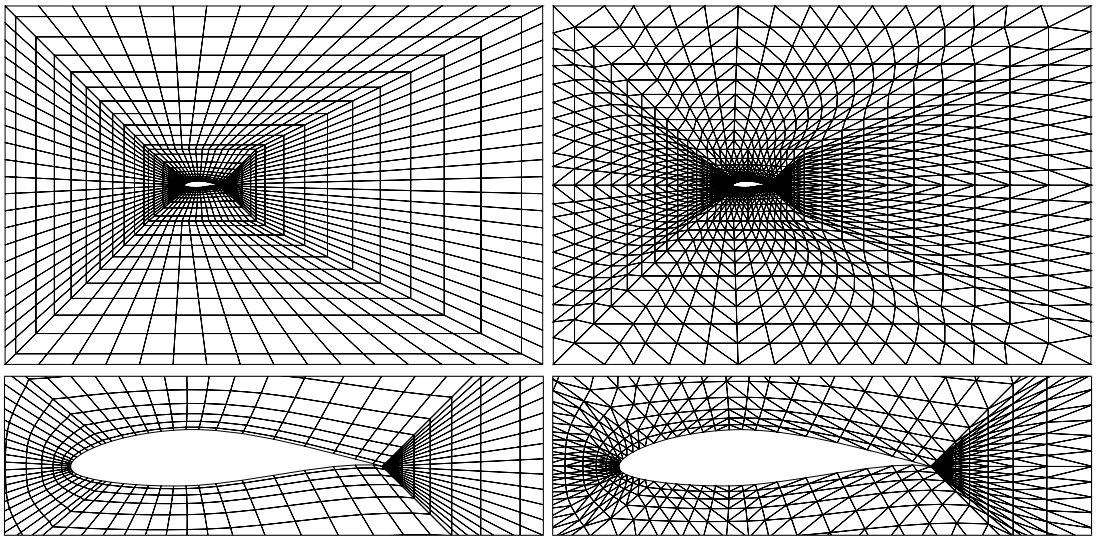

Figure 2: Left: Refined control mesh made of quadratic B-splines (1,681 control points and 1,400 elements). Right: Mesh made of linear finite elements (1,450 nodes and 2,780 elements).

		C_{D}	C_{L}
SUPS	Linear Finite Elements	0.0012	0.34
	Quadratic B-Splines	0.0044	0.41
VMST	Linear Finite Elements	0.0010	0.45
	Quadratic B-Splines	0.0032	0.52
Experimental Data From [22]		0.0050	0.45

Table 1: Drag and lift coefficients, C_{D} and C_{L}, for the computations and the measured values from [22].

flows. This multiscale technique is the space–time version of the variational multiscale method. We described the technique and presented results from test computations. These computations, and also the 3D computations [16] carried out using the technique, show that the technique is working well even with meshes that would normally be suitable for Reynolds-averaged Navier–Stokes (RANS) type computations. This justifies our expectation that the technique can also be used with meshes that would normally be suitable for a detached-eddy simulation (DES) type computation [23]. The same observation was made in [24] for the residual-based variational multiscale method using ALE and NURBS [15].

ACKNOWLEDGMENT

This work was supported by ARO Grant W911NF-09-1-0346. It was also supported in part by NSF Grant CRCNS-0903949, by NASA Grant NNX09AM89G, and by the Rice Computational Research Cluster funded by NSF Grant CNS-0821727.

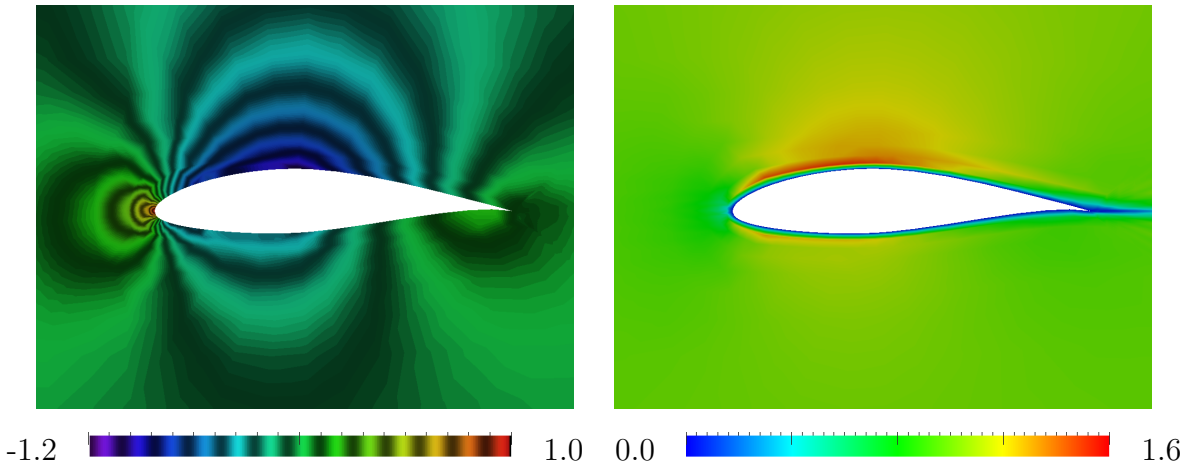

Figure 3: Computed with the DSD/SST-DP-SUPS technique and the mesh made of linear finite elements. Pressure coefficient (left) and velocity magnitude (right).

REFERENCES

[1] T.E. Tezduyar and S. Sathe, "Enhanced-discretization space-time technique (EDSTT)", *Computer Methods in Applied Mechanics and Engineering*, **193** (2004) 1385–1401.

[2] T.E. Tezduyar, M. Schwaab, and S. Sathe, "Sequentially-Coupled Arterial Fluid–Structure Interaction (SCAFSI) technique", *Computer Methods in Applied Mechanics and Engineering*, **198** (2009) 3524–3533.

[3] T.E. Tezduyar, K. Takizawa, C. Moorman, S. Wright, and J. Christopher, "Multiscale sequentially-coupled arterial FSI technique", *Computational Mechanics*, **46** (2010) 17–29.

[4] T.E. Tezduyar, K. Takizawa, C. Moorman, S. Wright, and J. Christopher, "Space–time finite element computation of complex fluid–structure interactions", *International Journal for Numerical Methods in Fluids*, **64** (2010) 1201–1218.

[5] K. Takizawa, S. Wright, C. Moorman, and T.E. Tezduyar, "Fluid–structure interaction modeling of parachute clusters", *International Journal for Numerical Methods in Fluids*, **65** (2011) 286–307.

[6] T.E. Tezduyar, "Stabilized finite element formulations for incompressible flow computations", *Advances in Applied Mechanics*, **28** (1992) 1–44.

[7] T.E. Tezduyar, "Computation of moving boundaries and interfaces and stabilization parameters", *International Journal for Numerical Methods in Fluids*, **43** (2003) 555–575.

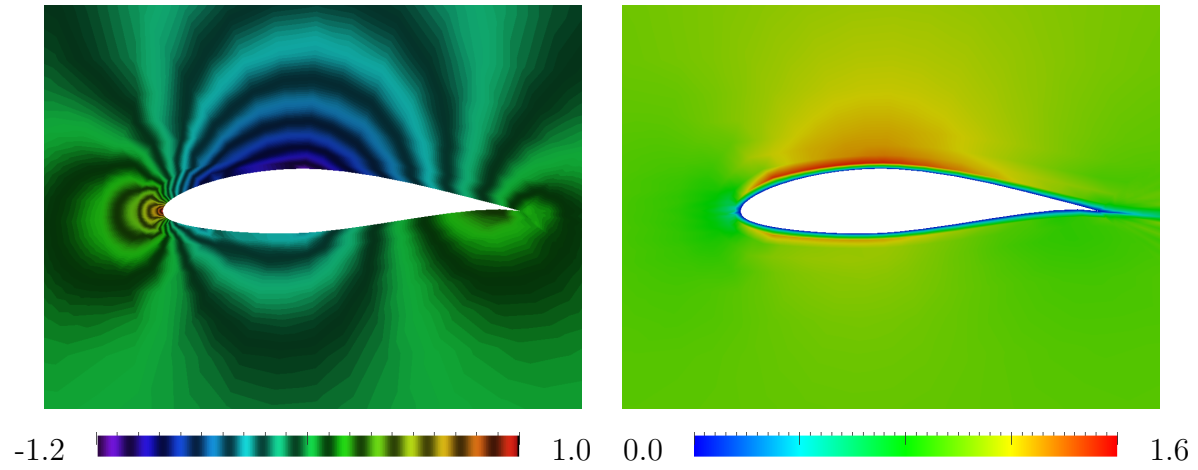

Figure 4: Computed with the DSD/SST-DP-VMST technique and the mesh made of linear finite elements. Pressure coefficient (left) and velocity magnitude (right).

[8] T.E. Tezduyar and S. Sathe, "Modeling of fluid–structure interactions with the space–time finite elements: Solution techniques", *International Journal for Numerical Methods in Fluids*, **54** (2007) 855–900.

[9] K. Takizawa and T.E. Tezduyar, "Multiscale space–time fluid–structure interaction techniques", *Computational Mechanics*, published online, DOI: 10.1007/s00466-011-0571-z, February 2011.

[10] T.J.R. Hughes, "Multiscale phenomena: Green's functions, the Dirichlet-to-Neumann formulation, subgrid scale models, bubbles, and the origins of stabilized methods", *Computer Methods in Applied Mechanics and Engineering*, **127** (1995) 387–401.

[11] T.J.R. Hughes, A.A. Oberai, and L. Mazzei, "Large eddy simulation of turbulent channel flows by the variational multiscale method", *Physics of Fluids*, **13** (2001) 1784–1799.

[12] T.J.R. Hughes and G. Sangalli, "Variational multiscale analysis: the fine-scale Green's function, projection, optimization, localization, and stabilized methods", *SIAM Journal of Numerical Analysis*, **45** (2007) 539–557.

[13] Y. Bazilevs, V.M. Calo, J.A. Cottrel, T.J.R. Hughes, A. Reali, and G. Scovazzi, "Variational multiscale residual-based turbulence modeling for large eddy simulation of incompressible flows", *Computer Methods in Applied Mechanics and Engineering*, **197** (2007) 173–201.

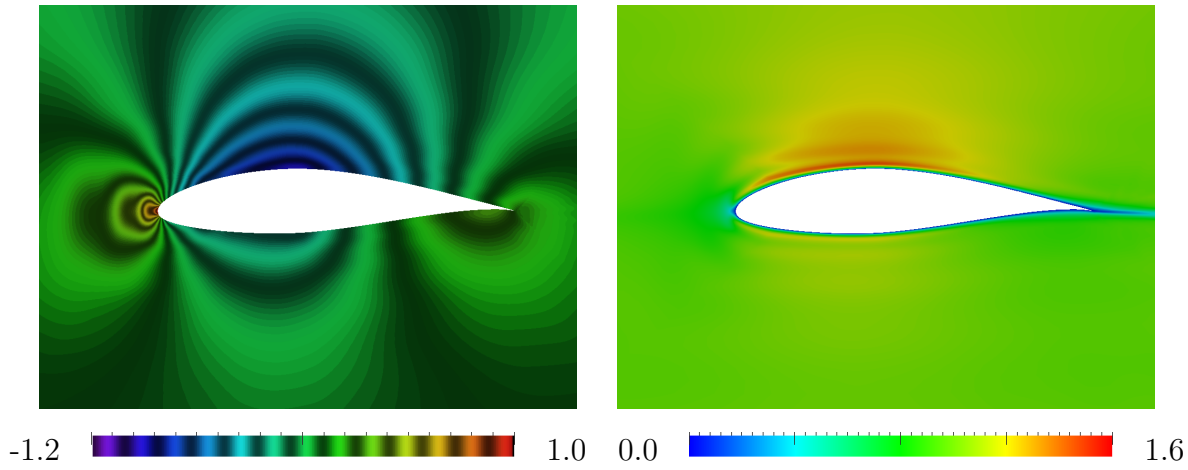

Figure 5: Computed with the DSD/SST-DP-SUPS technique and the mesh made of quadratic B-splines. Pressure coefficient (left) and velocity magnitude (right).

[14] Y. Bazilevs and I. Akkerman, "Large eddy simulation of turbulent Taylor–Couette flow using isogeometric analysis and the residual–based variational multiscale method", *Journal of Computational Physics*, **229** (2010) 3402–3414.

[15] Y. Bazilevs, M.-C. Hsu, I. Akkerman, S. Wright, K. Takizawa, B. Henicke, T. Spielman, and T.E. Tezduyar, "3D simulation of wind turbine rotors at full scale. Part I: Geometry modeling and aerodynamics", *International Journal for Numerical Methods in Fluids*, **65** (2011) 207–235.

[16] K. Takizawa, B. Henicke, T.E. Tezduyar, M.-C. Hsu, and Y. Bazilevs, "Stabilized space–time computation of wind-turbine rotor aerodynamics", *Computational Mechanics*, to appear, 2011.

[17] T.E. Tezduyar, M. Behr, and J. Liou, "A new strategy for finite element computations involving moving boundaries and interfaces – the deforming-spatial-domain/space–time procedure: I. The concept and the preliminary numerical tests", *Computer Methods in Applied Mechanics and Engineering*, **94** (1992) 339–351.

[18] T.E. Tezduyar, M. Behr, S. Mittal, and J. Liou, "A new strategy for finite element computations involving moving boundaries and interfaces – the deforming-spatial-domain/space–time procedure: II. Computation of free-surface flows, two-liquid flows, and flows with drifting cylinders", *Computer Methods in Applied Mechanics and Engineering*, **94** (1992) 353–371.

[19] T.E. Tezduyar and Y.J. Park, "Discontinuity capturing finite element formulations for nonlinear convection-diffusion-reaction equations", *Computer Methods in Applied Mechanics and Engineering*, **59** (1986) 307–325.

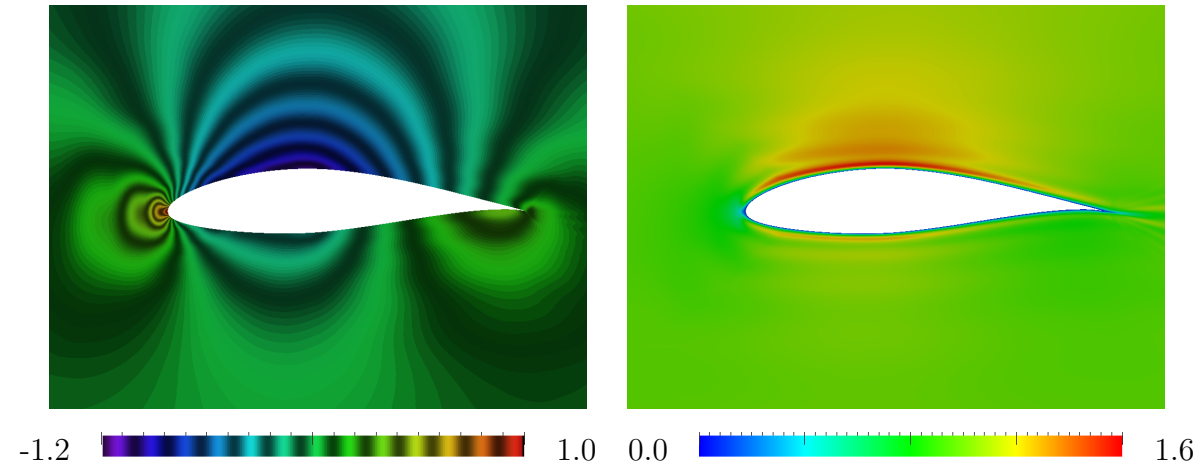

Figure 6: Computed with the DSD/SST-DP-VMST technique and the mesh made of quadratic B-splines. Pressure coefficient (left) and velocity magnitude (right).

[20] F. Shakib, T.J.R. Hughes, and Z. Johan, "A new finite element formulation for computational fluid dynamics: X. The compressible euler and navier-stokes equations", *Comput. Methods Appl. Mech. and Engrg.*, **89** (1991) 141–219.

[21] T.J.R. Hughes and A.A. Oberai, "Calculation of shear stress in Fourier–Galerkin formulations of turbulent channel flows: projection, the Dirichlet filter and conservation", *Journal of Computational Physics*, **188** (2003) 281–295.

[22] W.A. Timmer, "An overview of NACA 6-digit airfoil series characteristics with reference to airfoils for large wind turbine blades", in *Proceedings of AIAA 47th Aerospace Sciences Meeting*, AIAA Paper 2009-268, Orlando, Florida, (2009).

[23] P.R. Spalart, "Strategies for turbulence modelling and simulations", *International Journal of Heat and Fluid Flow*, (2000) 252–263.

[24] Y. Bazilevs, C. Michler, V.M. Calo, and T.J.R. Hughes, "Isogeometric variational multiscale modeling of wall-bounded turbulent flows with weakly enforced boundary conditions on unstretched meshes", *Computer Methods in Applied Mechanics and Engineering*, **199** (2010) 780–790.